Available online at www.sciencedirect.com

ScienceDirect

Procedia IUTAM 14 (2015) 246 – 255

Procedia IUTAM

www.elsevier.com/locate/procedia

IUTAM_ABCM Symposium on Laminar Turbulent Transition

Non-linear optimal perturbations in the asymptotic suction boundary-layer

Stefania Cherubini[a,*], Pietro De Palma[b], Jean-Christophe Robinet[a]

[a] *DynFluid Laboratory, Arts et Métiers ParisTech, 151 Bd. de l'Hopital, 75013 Paris, France*
[b] *DMMM, CEMeC, Politecnico di Bari, Via Re David 200, 70125 Bari, Italy*

Abstract

An asymptotic suction boundary layer (ASBL) flow is obtained when a given homogeneous suction is applied to a boundary-layer flow, highly stabilizing the flow with respect to Tollmienn-Schlichting waves. This work aims at verifying the stabilizing action of this homogeneous suction on linear and non-linear transition growth. Thus, the analytical ASBL solution is perturbed by optimal disturbances yielding the largest energy growth over a short time interval. Such perturbations are computed by a linear and *non-linear* global optimization approach based on a Lagrange multiplier technique. The results show that non-linear optimal perturbations are characterized by a localized basic building block, formed by staggered inclined vortices. In order to obtain a threshold amplitude for transition the optimization is coupled with a bisection of the perturbation initial energy, in order to compute the *minimal seed*, defined as the perturbation of minimal energy which lays on the frontier between the laminar and the turbulent states. This energy threshold is found to be 1 to 4 order of magnitude lower than the ones found by Levin et al. (2005) for other transition scenarios.

Selection and peer-review under responsibility of ABCM (Brazilian Society of Mechanical Sciences and Engineering)

Keywords:

Transition to turbulence; minimal seeds; non-linear coherent structures; hairpin vortices

1. Introduction

Despite many efforts in the last century, the origin of subcritical transition to turbulence in boundary-layer flows is still not very well understood. In particular, controlling, or at least delaying transition is still a very arduous task. Flow suction through the wall has been among the first techniques applied to control the structure of the boundary layer in order to reduce the drag[30]. The influence of suction on the stability of the boundary layer was studied by analytical methods considering uniform suction at wall. In particular, a very simple exponential solution for the velocity was derived by Meredith and Griffith (1938)[30] which would be valid at a sufficiently high distance from the leading edge of a flat plate. This solution of the Navier-Stokes equation is known as the asymptotic suction boundary layer (ASBL)[30] and is considered a suitable model to study boundary layers subject to active control by suction and to investigate the

* Corresponding author. Tel.: +33144246432.
E-mail address: s.cherubini@gmail.com

Selection and peer-review under responsibility of ABCM (Brazilian Society of Mechanical Sciences and Engineering)
doi:10.1016/j.piutam.2015.03.047

transition mechanism. In the 70's, Hocking[15] demonstrated that the critical Reynolds number is about two orders of magnitude higher than that of the Blasius boundary layer (BBL).

More recently, the development of the optimal transient growth analysis has renewed the interest in the study of the ASBL. In fact, it is well known that for a sufficiently high level of free-stream turbulence (FST), a bypass route to transition may occur in the boundary layer which corresponds to the growth of disturbances resembling the linear optimal perturbation (LOP)[25]. This mechanism is based on the development of streamwise-aligned structures composed by alternating low and high velocity streaks observed for the first time by Klebanoff[18]. The algebraic growth of the streaks due to the lift-up effect[20] leads eventually to secondary instability and break-up to turbulence[1]. Linear optimal perturbations, defined as those initial flow states yielding the largest amplification of the disturbance energy over a time/space interval through linear mechanisms, have been computed for many flows[3,23]. For the case of the boundary layer at low Reynolds number, such optimal structures consists of pairs of streamwise aligned counter-rotating vortices producing streamwise streaks by the lift-up effect, in perfect agreement with the above experimental findings. The same mechanisms have been studied in the ASBL. Fransson and Alfredsson (2003)[12] performed an experimental analysis about the algebraic growth of disturbances induced by free-stream turbulence. Using a local approach, Fransson and Corbett (2003)[13] computed LOP for the ASBL and compared their results with experiments. They observed a significant transient growth, although smaller than in the case of the BBL. This indicates that the strong effect of the damping of the energy growth obtained by suction for TS waves is not achieved in the case of the algebraic growth. Finally, Levin et al. (2005)[21] studied the energy thresholds for transition to turbulence in the ASBL, for $Re = 500,\ 800,\ 1200$, with perturbations having the form of oblique waves, streamwise vortices, or random noise; whereas, Levin et al. (2007)[22] analyzed the energy threshold for the same Reynolds numbers, in the case of localized disturbances, and investigated the formation and evolution of turbulent spots.

Very recently, a new technique has been developed for determining the minimum energy threshold to reach transition to turbulence in shear flows. In particular, it focuses on the computation of the minimum-energy perturbations confined on the boundary between the laminar and the turbulent states, called the *edge of chaos*[33,31,5,11]. Those perturbations can be very dangerous, being the closest ones to the laminar state capable of triggering transition. Concerning the ASBL, Kreilos et al.[19] investigated the structure of the edge of chaos and the relative attractors that live on it, identifying a periodic orbit embedded in the laminar-turbulent boundary[17], but they didn't look for the minimal energy states which may trigger transition. Very recently, the problem of finding the minimal energy perturbation on the edge of turbulence has been investigated by solving the non linear optimal growth problem for finite-amplitude initial perturbations (see Kerswell et al.[16] for a review). Those perturbations which optimize at a given (target) time the growth of a functional linked to transition (the kinetic energy or the dissipation for instance), called non linear optimal perturbations (NLOPs), have been found for a pipe flow[27,28]; a boundary layer flow[4,6]; and a Couette flow[26,29,8,11]. By optimizing the energy at large target times and bisecting the initial energy to bring the perturbation close to the laminar-turbulent boundary, the perturbation of minimal energy capable of bringing the flow to the edge state and then to transition, called the *minimal seed* of turbulent transition, can be found[29].

In all cases, the NLOPs are characterized by a very different structure with respect to the linear optimal ones and largely outgrow them in energy due to non linear mechanisms[6,28]. For the boundary-layer and the Couette flow, the NLOPs are characterized by a similar fundamental structure, composed of a localized array of vortices and low-momentum regions of typical length scale, capable of maximizing the energy growth most rapidly. Cherubini et al. (2011)[6,7] have discussed the contribution of non linear effects in such a strong energy growth, showing that non linearity is crucial to sustain the growth of such optimal perturbations. The knowledge of these non-linear mechanisms may allow one to design effective control strategies to delay transition by using wall suction[10]. The aim of the present paper is to extend the analysis of the NLOP to the case of the ASBL, following the approach that the authors have employed for the BBL, discussing similarities and differences between these two cases, and highlighting the role of the suction velocity.

The paper is organized as follows. In the second section we define the problem and describe the non linear optimization method. In the third section, a thorough discussion on non-linear optimal perturbations and their toute to transition is provided. Finaly, concluding remarks are provided.

2. Problem formulation

2.1. Governing equations and numerical method

The asymptotic suction boundary-layer flow is defined as the incompressible flow over a flat plate with a uniform wall-normal suction velocity V_S applied along the wall. The behaviour of an incompressible flow is governed by the Navier–Stokes (NS) equations:

$$\begin{aligned} &\frac{\partial \mathbf{u}}{\partial t} + (\mathbf{u}\cdot\nabla)\mathbf{u} = -\nabla p + \frac{1}{Re}\nabla^2\mathbf{u}, \\ &\nabla\cdot\mathbf{u} = 0, \end{aligned} \tag{1}$$

where $\mathbf{u} = (u, v, w)^T$ is the velocity vector and p indicates the pressure term. Dimensionless variables are defined with respect to the inflow boundary-layer displacement thickness δ^* and the freestream velocity, U_∞, so that the Reynolds number is $Re = U_\infty\delta^*/\nu$, ν being the kinematic viscosity. If a suction velocity of amplitude $V_S = 1/Re$ is imposed over the wall-normal direction y, and periodic conditions are used on the streamwise and spanwise directions, x and z, the following analytic solution is found[14]:

$$\mathbf{U} = ((1 - e^{-y}), -V_S, 0)^T. \tag{2}$$

On the base flow $\mathbf{U}$ given by the ASBL analytic solution, finite-amplitude perturbations have been superposed. The behaviour of these perturbations has been studied discretizing the NS equations (1) by a finite-difference fractional-step method[34], using a second-order-accurate centered space discretization. Performing a grid-convergence analysis, a mesh made up by $451 \times 100 \times 61$ points has been selected for the reference domain at $Re = 610$ with dimensions $L_x = 100$, $L_y = 20$ and $L_z = 10.5$. The spanwise dimension has been chosen very close to the one used in Ref.[21] for determining transition thresholds, whereas the streamwise length is much longer to avoid interaction of the flow structures with its own tail for long target times.

2.2. Non linear optimization

The non linear behavior of a perturbation $\mathbf{q} = (u', v', w', p')^T$ evolving in the laminar asymptotic suction boundary-layer flow is analyzed by solving the NS equations written in perturbative formulation with respect to the steady state solution, $\mathbf{Q} = (\mathbf{U}, P)^T$. A zero perturbation boundary condition is imposed for the three velocity components at the $y-$constant boundaries, whereas periodicity of the perturbation is forced in the spanwise and streamwise directions.

The goal is to find the perturbation at $t = 0$ providing the largest disturbance growth at a given target time, T. At this purpose, a Lagrange multiplier technique is used[27,4,24] to perform a constrained optimization of the perturbation energy. The disturbance energy density is defined as

$$E(t) = \frac{1}{2V}\int_V \left[u'^2(t) + v'^2(t) + w'^2(t)\right] dV = \frac{1}{2V}\left\langle \mathbf{u}'(t), \mathbf{u}'(t)\right\rangle, \tag{3}$$

where V is the volume of the computational domain. Given an initial energy $E(0) = E_0$, we aim at finding the shape and amplitude of an initial perturbation $\mathbf{q}_0$ which induces at target time T the largest energy gain $E(T)/E_0$; therefore, the objective function of the optimization procedure is $\mathfrak{I} = E(T)/E(0)$. The Lagrange multiplier technique consists in searching for extrema of an augmented functional, $\mathcal{L}$, with respect to every independent variable, the three-dimensional incompressible NS equations and the value of the initial energy being imposed as constraints. The augmented functional reads:

$$\begin{aligned} \mathcal{L} = \frac{E(T)}{E(0)} &- \int_0^T \left\langle \mathbf{u}^\dagger, \left\{ \frac{\partial \mathbf{u}'}{\partial t} - \mathbf{u}'\cdot\nabla\mathbf{U} + \mathbf{U}\cdot\nabla\mathbf{u}' + \mathbf{u}'\cdot\nabla\mathbf{u}' - \nabla p' - \frac{\nabla^2\mathbf{u}'}{Re} \right\} \right\rangle dt \\ &- \int_0^T \left\langle p^\dagger, \nabla\cdot\mathbf{u}' \right\rangle dt - \lambda\left(\frac{E_0}{E(0)} - 1\right). \end{aligned} \tag{4}$$

where $(\mathbf{u}^\dagger, p^\dagger, \lambda)$ are the Lagrange multipliers, e.g. the adjoint variables. Integrating by parts and setting to zero the first variation of $\mathcal{L}$ with respect to $(\mathbf{u}', p')$ leads to the adjoint equations plus the compatibility condition (which are

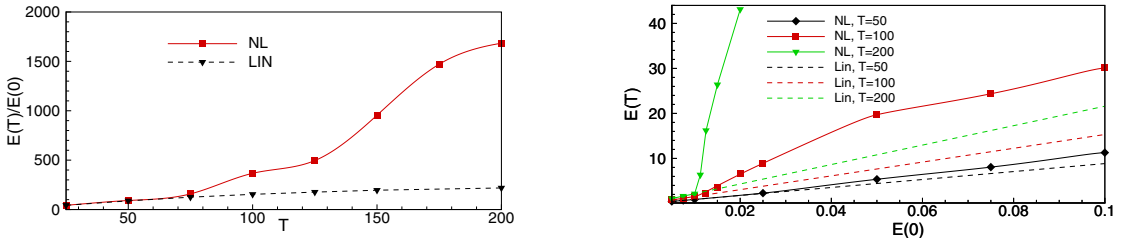

(a) (b)

Fig. 1. (a) Optimal energy gain versus target time T for $Re = 610$, $E_0 = 3.0 \times 10^{-7}$. The dashed line with triangles indicates the results of the linear optimization; the solid line with squares (red online) indicates the results of the non linear optimization. (b) Optimal energy for $Re = 610$ at target time $T = 50$ (black), $T = 100$ (red), and $T = 200$ (green) versus the initial energy $E(0)$, using the non linear optimization (solid lines with symbols) and the linear optimization (dashed lines).

provided in Ref.[6]). The gradient of the augmented functional with respect to the initial perturbation $\mathbf{q}_0$ is forced to vanish by means of a conjugate gradient algorithm as detailed in Ref.[6]. A coupled iterative approach is used to solve the problem, relying on the forward and backward solution of the direct and adjoint NS equations, respectively, and on the update of the initial perturbation in the conjugate gradient direction at each iteration, until convergence is reached. A detailed description of the optimization technique and of its convergence properties is provided in Ref.[6], for the case of the BBL flow, and in Ref.[8] for the Couette flow.

3. Results

3.1. Non linear optimal perturbations

The non linear optimization has been performed at Reynolds number $Re = 610$. This rather low Reynolds number (compared to the critical one for the ASBL) has been chosen for comparison purpose with the BBL case of Ref.[4]. Figure 1 (a) shows the value of the optimal energy gain versus the target time for an initial energy $E_0 = 3.0 \times 10^{-7}$. The dashed line refers to the results of a linear optimization, whereas the solid line represent the non linear optimization. As also observed for the BBL flow[4], the non linear optimal energy gain is remarkably larger than the corresponding linear one for $T > 50$. The influence of the parameter E_0 on the value of the optimal energy is shown in Figure 1 (b), for three values of the target time. It appears that a *non linearity threshold* value of the initial energy exists from which strong differences are observed in the non linear optimal energy with respect to the linear one (compare the solid lines with the dashed ones). Such a threshold decreases when the target time increases, as one can observe by comparing the solid lines in Figure 1 (b), converging towards a value, $E_0 = 1.2 \times 10^{-7}$, which might be close to the energy of the *minimal seed* for this Reynolds number (i.e., the perturbation of minimal energy on the laminar-turbulent boundary). Table 1 provides a comparison between the energy gains obtained for the BBL and the ASBL at $T = 75$ (the behavior is similar for different target times) for three optimizations: a linear optimization and two non linear optimizations with $E_0 = 1.2 \times 10^{-7}$ and $E_0 = 3.0 \times 10^{-7}$, respectively. The results indicate that a significant reduction of the optimal energy growth is obtained in the linear case; however, wall suction is much more effective in damping the growth of non linear optimal perturbations.

Crossing the non linearity threshold also yields large modifications in the shape of the optimal perturbations. This can be observed in Figure 2, which provides the optimal initial perturbations obtained for the ASBL at $Re = 610$ and $T = 75$, for two values of the initial energy, E_0. For the lowest one, $E_0 = 1.2 \times 10^{-7}$ (top frame), the perturbation is similar to that obtained by the linear optimization in a BBL flow[9], being characterized by alternated vortices elongated in the streamwise direction (black and white surfaces), localized in two different positions along the flat plate. Due to weak non linear effects, which are non-negligible for such values of the initial energy, some spanwise modulations are present on the streamwise perturbation (green surfaces). Concerning the amplitudes, the largest perturbation velocity component is the spanwise one ($|w_{max}| = 0.0027$), followed by the wall-normal ($|v_{max}| = 0.0025$) and the streamwise one ($|u_{max}| = 0.0003$). One can notice that the streamwise perturbation is one order of magnitude lower

Test case	Linear	$E_0 = 1.2 \times 10^{-7}$	$E_0 = 3.0 \times 10^{-7}$
BBL	275.10	801.98	1104.1
ASBL	125.16	125.15	158.37

Table 1. Comparison between energy gains at $T = 75$ for the BBL and the ASBL.

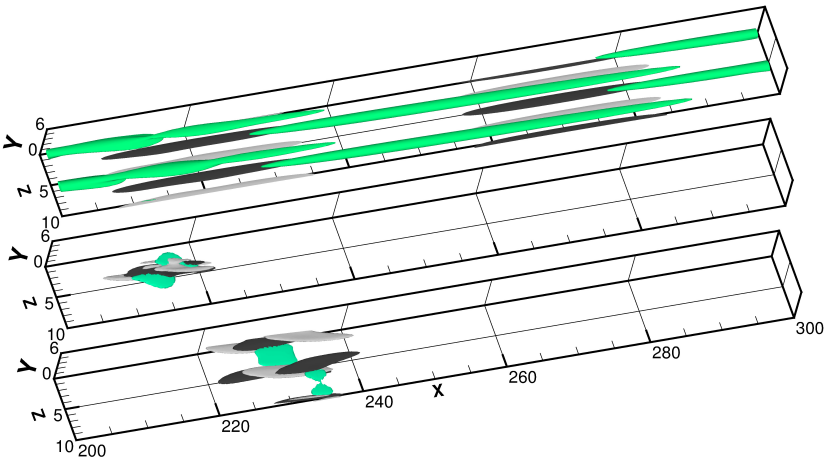

Fig. 2. (Color online) Initial perturbations obtained by the non linear optimization for the asymptotic suction boundary-layer at $Re = 610$ and target time $T = 75$: iso-surfaces of the optimal perturbations (grey, green online, for the negative streamwise component; dark and light gray for negative and positive streamwise vorticity, respectively) with initial energy $E_0 = 1.2 \times 10^{-7}$ (top frame, surfaces for $u' = -0.00017$, $\omega'_x = \pm 0.01$) and $E_0 = 3.0 \times 10^{-7}$ (middle frame, $u' = -0.015$, $\omega'_x = \pm 0.1$). Initial perturbations obtained by the non linear optimization for the Blasius boundary layer flow at $Re = 610$, target time $T = 75$, with initial energy $E_0 = 1.2 \times 10^{-7}$ (bottom frame, $u' = -0.01$, $\omega'_x = \pm 0.06$). Axes are not in the same scale.

than the others, meaning that for this value of the initial energy the mechanism of growth is still very close to the linear optimal one, based on the *lift-up* of the streamwise base flow velocity by the vortices given by the wall-normal and spanwise perturbation. However, as one can observe in figure 2, the shape of the optimal perturbation changes remarkably between $E_0 = 1.2 \times 10^{-7}$ and $E_0 = 3.0 \times 10^{-7}$. The most striking difference is the strong localization of the disturbance in both the streamwise and spanwise direction. For initial energies larger than the non linearity threshold, a strong localization of the initial perturbation leads to larger amplitudes (for the same initial energy), triggering non linear effects that induce a remarkable increase of the energy gain at target time. In fact, for an increase of the initial energy of a factor 2.5, we observe at $t = 0$ an increase of the velocity magnitudes of a factor of about 12 for v and w, whereas a factor 80 is obtained for u. These values of the perturbation velocity components, together with the particular shape of the disturbance, are able to trigger non linear effects which allow a much larger energy growth than in the linear case.

This strong localization appears to be a typical feature of NLOP in shear flows, since it has been also observed for the pipe[27,28], the BBL[6], and the Couette flow[26,8,29]. Furthermore, not only the extension, but also the structure of the perturbation changes remarkably. For $E_0 = 3.0 \times 10^{-7}$, the optimal perturbation is composed by three streamwise-alternated vortices showing a finite inclination with respect to the streamwise direction (black and white surfaces), whereas in the quasi-linear case at $E_0 = 1.2 \times 10^{-7}$ the vortices are streamwise-aligned. On both flanks of such inclined vortices, localized patches of finite-amplitude streamwise disturbance are observed (green surfaces). Concerning the relative magnitude of the velocity perturbations, the largest perturbation velocity component is the spanwise one ($|w_{max}| = 0.033$), followed by the streamwise ($|u_{max}| = 0.03$) and the wall-normal one ($|v_{max}| = 0.024$). These values are similar to those found for the Couette flow[8], whereas, for the BBL flow at the same Re, the largest component is the streamwise one, whose value is about half of the maximum value found here for the ASBL, for an initial energy just above the non linearity threshold, see Ref.[6]. It is worth noticing that, for all of these flows, in the linear case the streamwise velocity component at initial time is from one to two orders of magnitude lower than the spanwise and the

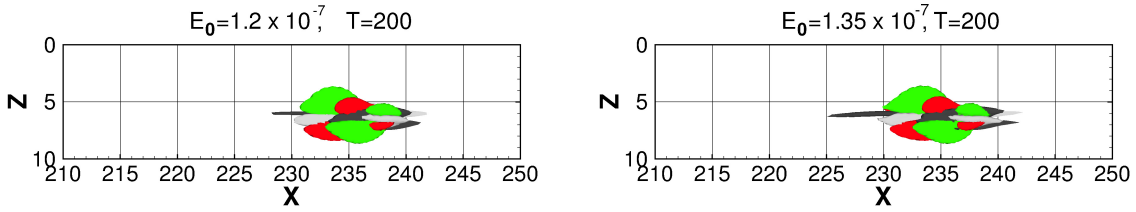

(a) (b)

Fig. 3. (Color online) Isosurfaces of the initial perturbations obtained by the non linear optimization for the ASBL at $Re = 610$ and target time $T = 200$, with initial energies $E_0 = 1.2 \times 10^{-7}$ (a), $E_0 = 1.35 \times 10^{-7}$ (b). Green and red, for the negative and positive streamwise velocity component; dark and light, for negative and positive streamwise vorticity, respectively, with values $u' = -0.005$, $\omega_x' = \pm 0.05$.

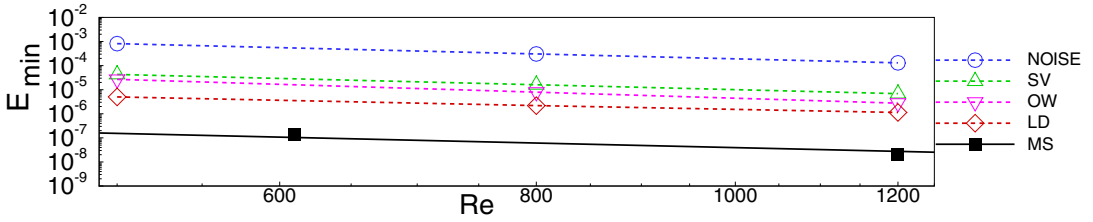

Fig. 4. Minimal energy for turbulent transition for the asymptotic suction boundary layer at different Reynolds numbers (solid line). The dashed lines show the minimal energy for different transition scenarios, namely noise (NOISE), streamwise vortices (SV), oblique waves (OW), and localized disturbances (LD), extrapolated from data in Ref.[22].

streamwise ones, whereas in the non linear case all of the components are of the same order, meaning that different mechanisms are responsible for the growth of the perturbation energy.

The structure of the NLOP found here shows some similarities with that found for the Couette flow (compare with Figure 5 of Ref.[8]) and with that obtained for the BBL flow (see Figure 2, bottom). However, while for the Couette and the ASBL flow (at least at low Reynolds number) the optimal disturbance does not show any particular symmetry, for the BBL it is symmetrical with respect to a $z = const$ axis. In fact, one can see in Figure 2 (bottom frame), that the NLOP for the Blasius flow at $E_0 = 1.2 \times 10^{-7}$ is composed by a basic structure similar to that of the ASBL, but the disturbance is symmetric with respect to a $z-$aligned axis.

As proposed in Ref.[27], the disturbance of minimum amplitude capable of triggering turbulence is defined as the *minimal seed* for a given Reynolds number. Bisecting the value of the initial energy at $T = 200$, and checking whether the obtained NLOP is able to induce transition, we have found the energy level of the minimal seed E_{min} to be about 1.277×10^{-7} for $Re = 610$. The corresponding maximum amplitudes of the velocity components are $|u|_{max} = 0.029, |v|_{max} = 0.031, |w|_{max} = 0.031$, very close to the values found at lower target time (even if the wall-normal component is now slightly larger than the streamwise one). The minimal seed is sandwiched between the NLOPs shown in figure 3 (a) and (b), for $E_0 = 1.2 \times 10^{-7}$ and $E_0 = 1.35 \times 10^{-7}$, both showing the basic structure provided in figure 2 (middle frame). It is worth to notice that the NLOP keeps the same structure of the minimal seed also for values of the initial energy slightly lower than the minimal seed energy.

The same analysis has been performed for a larger Reynolds number, $Re = 1200$, in order to generalize the results recovered at $Re = 610$, and to compare the energy thresholds with the computations performed in Refs.[21,22]. The solid line in Figure 4 shows the energy of the minimal seed, E_{min}, versus the Reynolds number, for $Re = 610, 1200$; whereas, the dashed lines in the figure reproduce the results of Ref.[21,22], for four different initial perturbation structures: i) random three-dimensional noise (NOISE); ii) streamwise vortices (SV), obtained by a local spatial optimization; iii) spatially extended oblique waves (OW), obtained by a local spatial optimization; iv) localized disturbances (LD) consisting of two alternated counter-rotating pairs of streamwise vortices. One can notice that the transition threshold provided by the minimal seed energy is amost two orders of magnitude lower than the energy thresholds found for spatially extended disturbances such as the streamwise vortices and the oblique waves. Moreover, E_{min} is one order

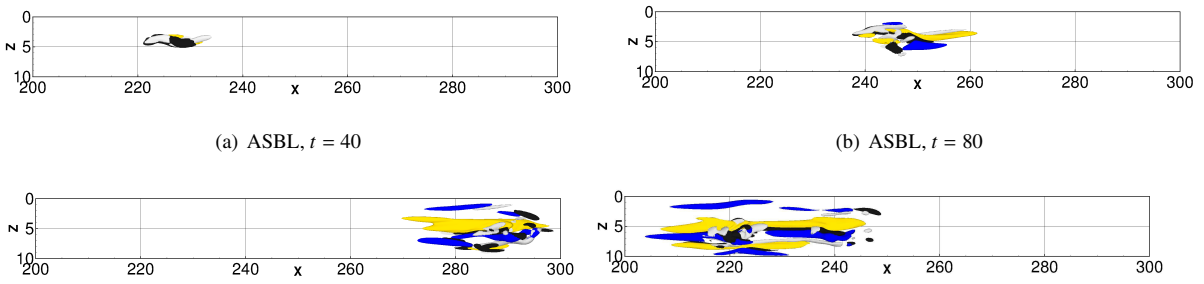

(a) ASBL, $t = 40$ (b) ASBL, $t = 80$

(c) ASBL, $t = 140$ (d) ASBL $t = 200$

Fig. 5. (Color online) Snapshots of the evolution in time of the selected NLOP for the ASBL: iso-surfaces of the streamwise velocity and vorticity perturbations (yellow and blue, for $u' = \pm 0.15$, respectively; black and white, $\omega'_x = \pm 0.2$, respectively) at $t = 40, 80, 140, 200$.

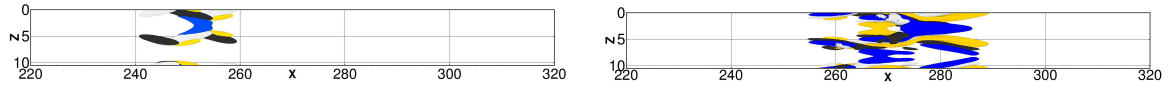

(a) BBL, $t = 40$ (b) BBL, $t = 80$

Fig. 6. (Color online) Snapshots of the evolution in time of the selected NLOP for the BBL: iso-surfaces of the streamwise velocity and vorticity perturbations (yellow and blue, for $u' = \pm 0.1$, respectively; black and white, $\omega'_x = \pm 0.2$, respectively) at $t = 40, 80$ (from left to right).

of magnitude lower than the minimal energy found for the localized perturbations selected in Ref.[22]. Concerning the velocity amplitudes, for $Re = 1200$ the minimal seed is characterized by $|u|_{max} = 0.014, |v|_{max} = 0.015, |w|_{max} = 0.017$. Whereas the minimal LD triggering transition in Ref.[22] was characterized by $|v|_{max} = 0.0124$, very close to the minimal amplitudes found here, but $|u|_{max} = 0.0$. Thus, the large difference in the transition thresholds can be linked on the complete absence of streamwise velocity disturbances in Ref.[22], which appears to be a crucial feature for inducing a rapid transition to turbulence using low-energy perturbations. Two other crucial elements which might explain the difference between the energy thresholds for the LD and the minimal seed are: i) the larger spatial extension of the LDs, which makes them more energetic than the minimal seed for similar associated amplitudes; ii) the fact that the vortices are perfectly aligned with the streamwise axis, and spanwise-symmetric with respect to this axis, whereas the perturbations inducing the largest growth by non linear mechanisms appear to be characterized by a finite inclination with respect to the streamwise axis, and do not show any spanwise symmetry. Thus, it appears that a non linear optimization is crucial to determine the order of magnitude of the minimal thresholds for transition to turbulence, and for accurately determining the shape and typical length scales of the minimal perturbation capable of inducing transition to turbulence.

The shape of the minimal seed for $Re = 1200$ is very similar to the ones described in the previous section for $Re = 610$. The persistence of this basic structure at different values of the initial energy, target times and for different kind of flows indicates that such a structure, which maximizes the disturbance energy over a finite time, has an intrinsic fundamental importance for shear flows.

3.2. The route of the non linear optimal perturbations to turbulence

In this section, we analyze by DNS the evolution towards turbulence of the NLOP obtained for the ASBL with $Re = 610$ and $T = 75$, providing a comparison with the NLOP of the BBL for the same conditions[6]. In order to achieve transition, the two perturbations have different energy, namely, $E_0 = 3.0 \times 10^{-7}$ for the ASBL and $E_0 = 1.2 \times 10^{-7}$ for the BBL.

A qualitative picture of the transition process initiated by the NLOP for the ASBL is given in figure 5, showing the streamwise vorticity (black and white surfaces) and velocity (blue and yellow) perturbations. At $t = 40$ (first frame), the initial vortices increase their strength and streamwise inclination. This first phase is similar to that found for the

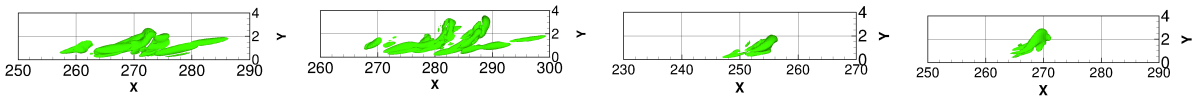

(a) BBL, $t = 80$ (b) BBL, $t = 100$ (c) ASBL, $t = 80$ (d) ASBL, $t = 100$

Fig. 7. (Color online) Snapshots of the evolution in time of the selected NLOP for the BBL (first and second frame) and for the ASBL (third and fourth frame). Isosurfaces of the Q criterion. .

BBL, and appears to depend on the action of non linear coupling terms linked to the components of the streamwise vorticity, such as ww_z, as explained in detail in Ref.[6]. At the same time, the streamwise velocity perturbation increases its amplitude, due to a *modified lift-up* effect[6]. In fact, since the initial vortices are inclined, the generated streaks are modulated in the streamwise direction, as shown in the second frame for $t = 80$. In particular, a main high-speed bent streak (yellow) is created, flanked by two weaker low-speed ones. On such streaks, localized patches of vorticity are observed (see the third frame for $t = 140$), which are originated from the splitting of the initial inclined vortices. The bent streaks continue to be fed by the streamwise vortices, elongating in the streamwise direction, as shown in the fourth frame for $t = 200$. However, in the regions of larger vorticity, stronger modulations of the streaks are induced, leading the wave packet to break-up starting from a localized region. Such a scenario recalls the mechanism of secondary instability of streamwise streaks which triggers bypass transition in boundary-layer flows[2,32]. In particular, since the initial disturbance is not symmetric, the streaks are characterized by sinuous oscillations, which represent the primary instabilities of streamwise streaks[1,2]. However, in the non linear optimal case, this mechanism is much more rapid than the one relying on the linear growth of streamwise-aligned streaks and successive saturation and secondary instability. In fact, the initial inclined vortices can create bent streaks in a short time, leading to break-up without experiencing secondary instability, due to their spanwise modulations[35]. The whole transition process recalls the first phases of the disturbance evolution on the periodic orbit recently found by bisection in a small domain (see Ref.[19]).

Despite the similarity of the initial optimal disturbances, the non linear route to transition described here shows important differences with respect to that found in the non-parallel case. In fact, for the BBL case, the perturbation maintains the initial symmetry of the NLOP up to large times (obviously, before turbulence is initiated). As shown in figure 6, the initial symmetric inclined vortices transport the flow momentum causing an amplification of the streamwise component of velocity along them and inducing the creation of low- and high-momentum zones showing a Λ and an X shape, respectively (see the blue and yellow surfaces in the first frame for $t = 40$). This Λ structure of the perturbation is maintained at larger time (see the second frame for $t = 80$), and the symmetric inclined vortices connect their fronts to create a $\Lambda-$vortex, which eventually turns into a hairpin vortex which leads the flow to break-up. The formation of the hairpin for the BBL can be clearly seen in figure 7 at times $t = 80$ and $t = 100$, where the green surfaces show the Q-criterion, highlighting the regions of high vorticity. The vortices in the heart of the wave packet increase their inclination, reaching angles of about 35°. This phase coincides with the formation of the hairpin vortex (two of them are visible in the second frame at $t = 100$) which grows in size and splits into smaller hairpin vortices, leading very quickly to a turbulent spot. On the other hand, for the ASBL, although the initial vortices show a similar wall-normal inclination with respect to the streamwise direction, as shown in the third and fourth frame of figure 7, the head of the hairpin vortex cannot be created. Thus, the vorticity does not spread in space as in the BBL case, but remains localized in a narrow region in the streamwise direction (see the fourth frame at $t = 100$).

The differences between the transition paths in the ASBL and BBL case can be analyzed by extracting the rms values of the three components of the velocity perturbation, as shown in figure 8, the thick lines referring to the ASBL, the thin ones to the BBL. In the BBL flow, the three components of velocity grow more rapidly and achieve larger rms values than in the ASBL case (see figure 8 (a)). Concerning the vorticity perturbation, shown in figure 8 (b), in the BBL case all of the three components grow more rapidly; the largest differences between the two flows are recovered for the wall-normal and spanwise vorticity, which attains values almost one order of magnitude larger than in the ASBL case. This can be explained by observing that the vorticity components ω'_z and ω'_y have large values at the head and legs of the hairpin which characterize the BBL route to transition. In fact, plotting the ω'_z and ω'_y surfaces for the parallel and non-parallel flow cases at $t = 100$, as provided in figure 9 (a) and (b), respectively, one can observe that these two components of the vorticity perturbations are much more extended in space, and

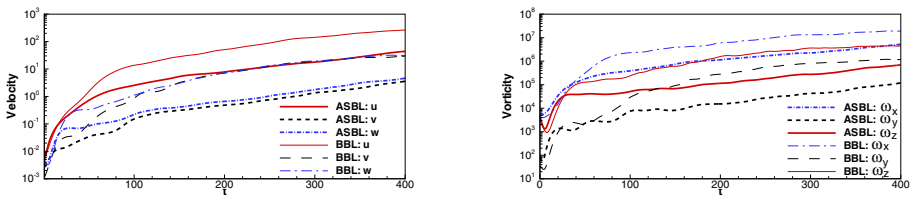

(a) (b)

Fig. 8. (Color online) Evolution in time of the rms values of the three components of velocity (solid lines for u', dashed for v', dashed-dotted for w') (a) and vorticity (solid lines for ω'_z, dashed for ω'_y, dashed-dotted for ω'_x) (b) for a DNS initialized by the selected NLOP for the ASBL (thick lines) and the BBL (thin lines).

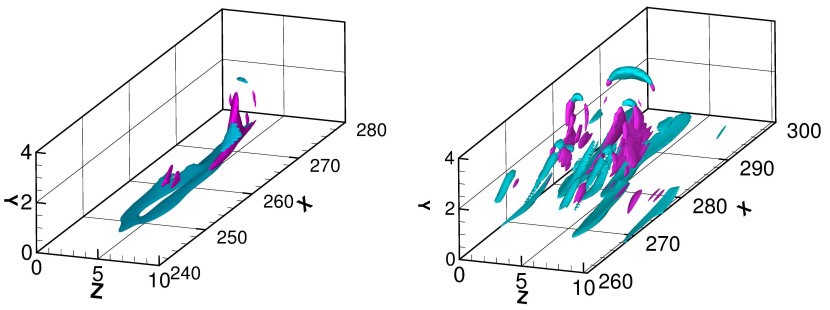

Fig. 9. (Color online) Snapshots of the evolution in time of the selected NLOP for the ASBL (left frame) and the BBL (right frame): spanwise and wall-normal vorticity (blue surfaces for $\omega'_z = 0.8$, red ones for $\omega'_y = 0.65$.

larger in magnitude in the non-parallel case than in the parallel one (both components are about 30%). In particular, the vorticity surfaces are localized at the head and legs of the hairpin vortices, explaining the larger growth of such terms with respect to the streamwise vorticity. This explains the difference between the transition scenarios in the two different flows, and the crucial effect of considering both non-parallelism and non-linearity in the computation of optimal perturbations.

4. Summary

A variational procedure has been employed to find *non linear* optimal disturbances in the asymptotic suction boundary layer (ASBL) flow. These perturbations are defined as the ones yielding the largest energy growth at a given target time T, for a given Reynolds number Re. The results have been compared with those obtained using the same approach in the case of the Blasius boundary layer (BBL) flow[4]. It has been found that suction remarkably reduces the optimal energy gain in the non linear case. Moreover, the optimal perturbation obtained in the present case shares the same basic structure found for different shear flows such as the BBL and the Couette flows. However, unlike the BBL case, the optimal perturbation for the ASBL flow is not spanwise-symmetric. By bisecting the initial energy of the non linear optimal perturbations, minimal energy thresholds for subcritical transition to turbulence have been obtained. These energy thresholds are found to be 1 to 4 order of magnitude lower than the ones found in other transition scenarios such as secondary instability of elongated streamwise vortices, random noise, oblique waves and localized streamwise-aligned disturbances[21]. Finally, direct numerical simulations show that the different structure of the base flow with respect to the BBL leads to a different evolution of the initial perturbation. In fact, unlike the case of the BBL flow, the formation of hairpin vortices is not observed in the transition process before break-up to turbulence, and a sinuous transition scenario is observed. This appears to be due to the lower tilting of the vortices induced by the fuller velocity profile in the ASBL case, which delay the formation of hairpin vortices.

Acknowledgments

Some computations have been performed on the IBM x3750-M4 of the IDRIS, France, under grant i20142a2188.

References

1. P. Andersson, L. Brandt, A. Bottaro, and D. S. Henningson. On the breakdown of boundary layer streaks . *J. Fluid Mech.*, 428:29–60, 2001.
2. L. Brandt, P. Schlatter, and D. S. Henningson. Transition in a boundary layers subject to free-stream turbulence . *J. Fluid Mech.*, 517:167–198, 2004.
3. K. M. Butler and B. F. Farrell. Three-dimensional optimal perturbations in viscous shear flow . *Phys. Fluids A*, 4:1637–1650, 1992.
4. S. Cherubini, P. De Palma, J.-Ch. Robinet, and A. Bottaro. Rapid path to transition via nonlinear localized optimal perturbations . *Phys. Rev. E*, 82:066302, 2010.
5. S. Cherubini, P. De Palma, J.-Ch. Robinet, and A. Bottaro. Edge states in a boundary layer . *Phys. of Fluids*, 23:051705, 2011.
6. S. Cherubini, P. De Palma, J.-Ch. Robinet, and A. Bottaro. The minimal seed of turbulence transition in a boundary layer . *J. Fluid Mech.*, 689:221–253, 2011.
7. S. Cherubini, P. De Palma, J.-Ch. Robinet, and A. Bottaro. A purely nonlinear route to transition approaching the edge of chaos in a boundary layer . *Fluid Dynamics Research*, 44:031404, 2012.
8. S. Cherubini and De Palma. Nonlinear optimal perturbations in a Couette flow: bursting and transition . *J. Fluid Mech.*, 716:251–279, 2012.
9. S. Cherubini, J.-Ch. Robinet, A. Bottaro, and P. De Palma. Optimal wave packets in a boundary layer and initial phases of a turbulent spot . *J. Fluid Mech.*, 656:231–259, 2010.
10. S. Cherubini, J.-Ch. Robinet, and P. De Palma. Nonlinear control of unsteady finite-amplitude perturbations in the Blasius boundary-layer flow . *J. Fluid Mech.*, 737:440–465, 2013.
11. Y. Duguet, A. Monokrousos, L. Brandt, and D. S. Henningson. Minimal transition thresholds in plane Couette flow . *Phys. Fluids*, 25:084103, 2013.
12. J. H. M. Fransson and P. H. Alfredsson. On the disturbance growth in an asymptotic suction boundary layers . *J. Fluid Mech.*, 482:51–90, 2003.
13. J. H. M. Fransson and P. Corbett. Optimal linear growth in the asymptotic suction boundary layer . *Eur. J. Mech./Fluids*, 22:259–270, 2003.
14. A. A. Griffith and F. W. Meredith. The possible improvement in aircraft performance due to boundary layer suction. *Rep. Aero. Res. Coun.*, Tech. Rep., 1936.
15. L. M. Hocking. Non-linear instability of the asymptotic suction velocity profile . *Q. J. Mech. Appl. Maths*, 28:341–353, 1975.
16. R. R. Kerswell, C. C. T. Pringle, and A. P. Willis. An optimisation approach for analysing nonlinear stability with transition to turbulence in fluids as an exemplar . *Rep. Prog. Phys.*, 77:085901, 2014.
17. T. Khapko, T. Kreilos, P. Schlatter, Y. Duguet, B. Eckhardt, and D. Henningson. Localized edge states in the asymptotic suction boundary layer . *J. Fluid Mech.*, 717:R6, 2013.
18. P. S. Klebanoff. Effects of freestream turbulence on the laminar boundary layer . *Bull Am. Phys. Soc.*, 10(1323), 1971.
19. T. Kreilos, G. Veble, T. M. Schneider, and B. Eckhardt. Edge states for the turbulence transition in the asymptotic suction boundary layer . *J. Fluid Mech.*, 726:100–122, 2013.
20. M. T. Landahl. A note on an algebraic instability of inviscid parallel shear flows . *J. Fluid Mech.*, 98:243–251, 1980.
21. O. Levin, N. Davidsson, and D. S. Henningson. Transition thresholds in the asymptotic suction boundary layer . *Physics of Fluids. A, Fluid Dynamics*, 17:114104, 2005.
22. O. Levin and D. S. Henningson. Turbulent spots in the asymptotic suction boundary layer . *J. Fluid Mech*, 548:397–413, 2007.
23. P. Luchini. Reynolds number indipendent instability of the Blasius boundary layer over a flat surface: optimal perturbations . *J. Fluid Mech.*, 404:289–309, 2000.
24. P. Luchini and Bottaro. Adjoint Equations in Stability Analysis . *Ann. Rev. Fluid Mech.*, 46:493–517, 2014.
25. M. Matsubara and P.H. Alfredsson. Disturbance growth in boundary layers subjected to free-stream turbulence . *J. Fluid Mech.*, 430:149–168, 2001.
26. A. Monokrousos, A. Bottaro, L. Brandt, A. Di Vita, and D. S. Henningson. Non-equilibrium thermodynamics and the optimal path to turbulence in shear flows . *Phys. Rev. Lett.*, 106:134502, 2011.
27. C. C. T. Pringle and R.R. Kerswell. Using nonlinear transient growth to construct the minimal seed for shear flow turbulence . *Phys. Rev. Lett.*, 105:154502, 2010.
28. C. C. T. Pringle, A. Willis, and R.R. Kerswell. Minimal seeds for shear flow turbulence: using nonlinear transient growth to touch the edge of chaos . *J. Fluid Mech.*, 702:415–443, 2011.
29. S.M.E. Rabin, C. P. Caulfield, and R.R. Kerswell. Triggering turbulence efficiently in plane Couette flow . *J. Fluid Mech.*, 712:244–272, 2012.
30. H. Schlichting. Boundary layer theory . *Springer*, 2004.
31. T. M. Schneider, B. Eckhardt, and J.A. Yorke. Turbulence Transition and the Edge of Chaos in Pipe Flow . *Phys. Rev. Lett.*, 99:034502, 2007.
32. W. Schoppa and F. Hussain. Coherent structure generation in near-wall turbulence . *J. Fluid Mech.*, 453:57–108, 2002.
33. J. D. Skufca, J.A. Yorke, and B. Eckhardt. Edge of chaos in a parallel shear flow . *Phys. Rev. Lett.*, 96:174101, 2006.
34. R. Verzicco and P. Orlandi. A finite-difference scheme for the three-dimensional incompressible flows in cylindrical coordinates . *J. Comp. Phys.*, 123(2):402–414, 1996.
35. F. Waleffe. On a self-sustaining process in shear flows . *Phys. Fluids*, 9:883–901, 1997.